COST CA 19111

European Network on Future Generation Optical Wireless Communication Technologies (NEWFOCUS)

Deliverable D1.2

Proof of Concept Demonstrators

Date: 28/05/2024

Edited By:

Luis Nero Alves (Instituto de Telecomunicações, Aveiro, Portugal)

Pranciskus Vitta (Vilnius University, Faculty of Physics, Lithuania)

This document is based upon work from COST Action NEWFOCUS, supported by COST (European Cooperation in Science and Technology)

List of contributors

Name	Country
Erich Leitgeb	AT
George-Iulian Uleru	RO
Gurgen Mardoyan	AM
Hovik Baghdasaryan	AM
Carlos Morales	SP
Yongtao Qu	UK
Juan Zafra	SP
Iñaki Martinez-Sarriegui	SP
José Sánchez-Pena	SP
Luis Nero Alves	PT
Luis Rodrigues	PT
Marian Marciniak	PL
Mircea Hulea	RO
Mónica Figueiredo	PT
Othman Younus	UK
Sujan Rajbhandari	UK
Tamara Hovhannisyan	AM
Tamara Knyazyan	AM
Tigran Baghdasaryan	BE
Zabih Ghassemlooy	UK

This document is based upon work from COST Action NEWFOCUS, supported by COST (European Cooperation in Science and Technology)

1. Introduction

As part of NEWFOCUS network, WG1 - Ultra-short-range links has the overall goal to develop Point-to-Point and high performance Optical Wirelesss communications OWC based solutions for ultra-high-speed links for sub-metre applications. Towards this goal the major tasks are: T1.1- Channel modelling and characterization for application oriented scenarios with particular focus on optical front-end characteristics; T1.2- Design of innovative PHY layer solutions including MIMO structures; T.1.3- Upper layer design coping with QoS constraints and T1.4- Design and assessment of compact, energy-efficient and high-performance PoC demonstrators for optical interfaces and short-range high data-rate VLC systems. For the current reporting period, deliverable D1.2 on proof of concept demonstrators, reports the major findings communicated by the MC members contributing to this group.

2. State of the art

WG1 focuses on the transmission of sub-meter communication links, such as intra- and inter-chip communication, high-performance computing platforms, and device-to-device communication in dense IoT scenarios. Recent research has shown that OWC is a promising technology for these types of scenarios. Free space optical (FSO) interconnects, such as FSOIs in integrated circuit and printed circuit board designs, provide higher speeds with low energy consumption per bit compared to metal interconnects. Optical devices, including multiple quantum well modulators/detectors and vertical cavity surface-emitting lasers (VCSELs), have been proposed as solutions for inter-chip connectivity [1]. FSOIs offer several advantages, such as higher capacity and design flexibility, mitigation of routing and switching issues, and reduced electromagnetic interference. They can also be used in high-performance computing platforms and intra-satellite systems. However, there is a lack of focused research direction in this field, and several scientific and technical issues need to be addressed, such as beam wandering and occlusion due to temperature effects and dust-induced signal dispersion, as well as cross-link interference with wavelength reuse in line-of-sight and/or diffused optical transmission configurations. While wavelength division multiplexing and multiple-input multiple-output techniques have been explored to increase data throughput at the physical layer, there have not been many reported research works on media access control and upper network protocol layers. OWC also presents unique opportunities for short-range, hyper-dense IoT applications that require reliable connections between smart objects with sensing/actuating and communication capabilities. RF technologies may struggle with these requirements, making OWC an attractive option. Ongoing research is focusing on establishing reliable OWC links for low-power, resource-constrained devices, mobility issues such as fast pointing and fading mitigation, and inexpensive and seamless integration of transmitters (Txs) and receivers (Rxs) in wireless sensor-based infrastructure.

3. Recent achievements

The following sections report the recent achivemnst on WG1 arising from input document contributions by MC mebers showing interest in WG1. Contributions focus On the targeted goals for the reporting period, aiming at contributions on channel modeling and PHY layer design considerations, respectively, Tasks T1.1, T1.2 and T1.4. Sections 3.1 to 3.5 report transceiver architectures for focused pplications. In 3.1 it is reported the PHY layer tarnceiver design for chip-to-chip interconnects. In 3.2 it is reported a system architecture for IoT dense scenarios using visible light

This document is based upon work from COST Action NEWFOCUS, supported by COST (European Cooperation in Science and Technology)

communications supported on M-CAP, the work reports on PHY and MAC layer design aiming at frame synchronization. In 3.3 it is reported a neuromorphic architecture for sensing using visible light communications. The work on 3.4 reports on findings on using perovskite photovoltaic cells as optical recievers. Finally the work in 3.5 reports on a spiking neural network (SNN) using PAM modulation scheme and visible light as communication medium. All the works reported are in the form of proof of concept demonstrators, thus requiring a system implementation and experimental verification.

3.1. Wavelength-scale modelling of transmissive and reflective type multi-nanolayer electro-optical modulators for chip-to-chip free space optical interconnection

We studied modulating characteristics of transmissive and reflective Fabry-Perot type multi-nanolayer conductor-dielectric electro-optical modulators (EOMs) for chip-to-chip free space optical interconnection using wavelength-scale electromagnetic modelling. For the analysis we used frequency-domain method of single expression (MSE). As shown in Fig. 1, the considered EOM structures consist of an electro-optical spacer of LiNbO3 covered by two thin ITO conducting nano-layers, surrounded by Si/SiO2 distributed Bragg reflectors (DBRs). In the case of transmissive EOM the DBRs are symmetric regarding the spacer, while in the case of reflective EOM they are asymmetric to provide high reflectance for the structure. From four possible types of DBRs the suitable structure has been chosen with layers of higher permittivity adjoining to the ITO nano-layers. ITO nano-layers serving as electric contacts for supplying modulating electrical signal to the electro-optical spacer are parts of the multi-nanolayer structure and included in the electromagnetic model.

We assumed incident radiation from an external laser diode at 1.55 µm wavelength. The optimal configurations of the EOM structures providing a high peak in the transmittance for the transmissive EOM and a narrow dip in the reflectance for the reflective EOM are proposed. Efficiency of optical wave intensity modulation is analysed by means of influence of electro-optical spacer's permittivity change on the transmittance and the reflectance of the EOM structures.

Recently, we have also extended our study to model spatial hole burning effects in reflective type EOMs. Spatial hole burning is a well-known nonlinear effect of longitudinal gain modulation, which decreases amplifying abilities of such amplifiers. Unlike many other approaches reported in literature, when approximation or weak nonlinearities are assumed to address the phenomenon, owing to the inverse propagation approach used in method of single expression we were able to model this non-linear effect with high numerical accuracy and without approximations. The reflectance decrease of EOMs is stipulated by gain modulation. The modeling results taking into account the non-linear gain modulation are presented in Fig. 2.

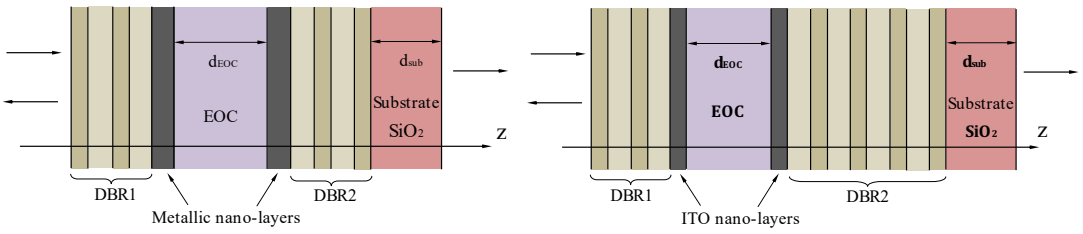

3) b)

Figure1. Transmissive (a) and reflective (b) type multi-nanolayer Fabry-Perot EOMs at the normal incidence of optical wave from the left.

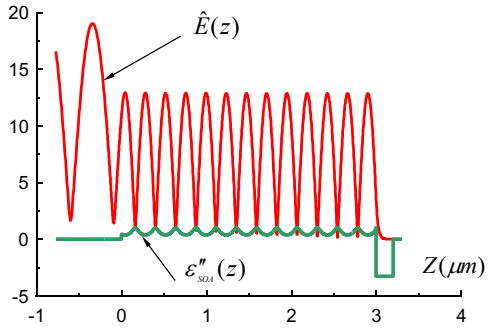

Figure 2. Distribution of electric field amplitude $\hat{E}(z)$ and modulated gain $\varepsilon''_{SOA}(z)$.

Obtained distribution for the longitudinal spatial hole burning within the amplifying part of the EOM indicates a strong correlation with the semi-standing optical wave pattern within the amplifying structure.

3.2 Visible Light Communication Systems Architectures for the Internet of Things

SYSTEM ARCHITECTURE

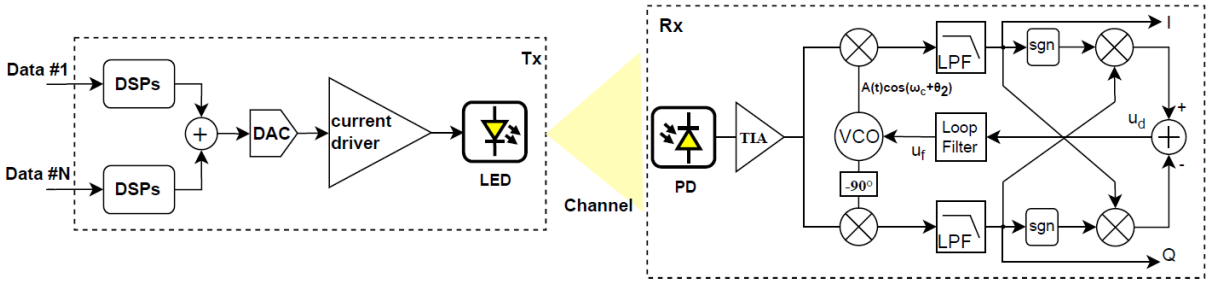

Figure 3 – System architecture of the digital m-CAP Tx and the VLC analogue Rx.

Aiming at low-cost, low-power, and compact IoT devices, the proposed architecture makes use of analogue Rxs and a digital m-CAP modulator fitted in a ceiling LED light fixture. A digital m-CAP modulator performs the modulation of all the bands, while in the Rx side a homodyne Rx is used to demodulate a single band, as seen in Figure . The modulated spectrum was divided into 100 bands, with a total bandwidth of 1 MHz, which can be seen as a frequency division multiple access scheme (FDMA). Nevertheless, typical lighting LEDs have a modulation bandwidth up to 3 MHz, and if considering narrow-band communications, the number of bands can be easily scaled up. Therefore, each band of the proposed system has a bandwidth of 5 kHz, with a throughput of 10 kbit/s. The system performance was assessed with multiple combinations of emitter and Rx filters – the digital m-CAP modulator pulse shaping filter $p(t)$ considered a raised cosine filters as well as digital matched filters for the analogue Bessel and Butterworth filters [4]. When considering guard bands, Bessel filters presented a bit error rate (BER) performance with a 0.5 dB Eb/No gain loss when compared to the theoretical QAM modulation BER curve in the presence of AWGN. Moreover, the proposed architecture could achieve a BER lower than 10^{-3} for an energy-to-noise ratio (Eb/No) of 6 dB using a third-order analogue Bessel filter and a properly synchronized quadrature mixer. A mixed solution combining FDMA and TDMA can be considered for increasing the device number capacity, by time

This document is based upon work from COST Action NEWFOCUS, supported by COST (European Cooperation in Science and Technology)

alternating adjacent bands – although the devices throughput lowers to one half, the network can accommodate the double of devices.

EXPERIMENTAL FRONTEND AND MODULATION RESULTS

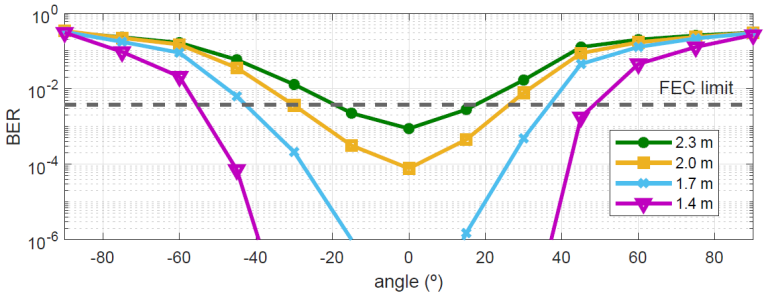

Figure 4 - BER vs. Tx angle ∈ [−90◦, 90◦] for a range of d.

To experimentally validate the proposed architecture, a LED driver (with a 1 W LED) and the analogue Rx were implemented, and the eye patterns, Rx constellations, error vector magnitude (EVM), and BER were obtained [5]. Here, BER vs. distance and the BER vs. The Tx/Rx angle LOS scenarios were considered. As can be seen in Figure , the BER performance is resilient in the presence of Tx/Rx misalignment, particularly for shorter distances where the device tilt can go as high as 45° and still achieve a BER within the forward error correction (FEC) limit. The result is particularly significant given that typical LED lighting fixtures often have a larger radiation pattern, which minimizes the impact of Tx/Rx misalignment in real-world scenarios. An improved SNR is expected in testbeds based on commercial lighting fixtures since the LED utilized in the experimental validation is rated at 1 W, which has a lower power when compared to the power ratings of the current lighting systems.

CARRIER RECOVERY

The carrier synchronization of homodyne Rxs is a critical aspect in real-world implementations because of imperfections of devices, as well as the channel delays and interferences. Using the MatLab Simulink, a simulation model for the Costas Loop was developed in order to validate the system's ability to synchronize. Pull-in and lock ranges of ±800 Hz and ±900 Hz were obtained, respectively, requiring 1.194 ms to be in the locked state, correspondent to less than 6 symbols period. Furthermore, we analyse the system's performance while facing noise and interference from other modulated bands. A comparison with the ideal synchronization scenario revealed that the presence of noise and interference did not negatively impact the EVM [6]. However, the system presented issues when energy was present in adjacent bands. Nonetheless, there are potential solutions to enhance the system's performance without substantially increasing device requirements, including a high order phase-locked loop and a hybrid FDMA/TDMA.

DATA CLOCK RECOVERY

The synchronization of data clocks between the Tx and the Rx is a critical aspect of data communication systems, ensuring accurate and reliable data transmission since it can avoid timing errors, packet loss, and data corruption. The issue may arise from the clock source misalignment between the Tx and the Rx due to the electronic devices' precision, and voltage and temperature dependence, as well as from the channel propagation delay. We proposed and demonstrated a data clock synchronization scheme with a VLC frame-based transmission protocol using a hybrid m-CAP/QAM modulation compatible with IoT applications requirements. The proposed method considers the usage of encapsulated data

This document is based upon work from COST Action NEWFOCUS, supported by COST (European Cooperation in Science and Technology)

symbols in data packets, allowing a simple Rx device featuring a low cost microcontroller to recover the data clock at the beginning of each frame and correctly sampling the transmitted data until the end of the packet. This method can use oversampled digital data to find the optimum sampling time, discarding the usage of the high-speed analod-to-digital convertors (ADCs). However, this method does not eliminate the clock frequency misalignment and the Tx and Rx clocks will eventually skew after some time, dependant on the misalignment magnitude. Nevertheless, the maximum misalignment can be estimated from the precision and temperature drift of the clock generators that are being used in the Tx and the Rx. From the experimental results, we saw that the time misalignment between I and Q, i.e. jitter, which appears due to ISI, plays a major issue in the proposed algorithm. An extra step was implemented in the recovery algorithm in order to accommodate the experimental setup jitter, which includes a tolerance of two samples, about 20% of the total symbol period, to correctly recover the data clock.

CONCLUSIONS

This work demonstrates the viability of potentially low-cost, low-power solution for VLC-based IoT systems, using a digital m-CAP Tx and an analogue QAM Rx. In one hand, the experimental results validate that we could successfully demodulate only one band, without the need of high capability DSPs. On the other hand, the carrier synchronization demonstrated that the most adequate multiple access scheme is a hybrid FDMA/TDMA. Suitable applications for this system may include actuators control in Industrial IoT, smart indoor farming, and retail inventory management (smart shelf labels).

3.3 Neuromorphic sensors with VLC

Spiking neural networks (SNN) can control single-joint robotic arms' precise rotation and force when shape memory alloy (SMA) actuators are used. For the purpose of controlling anthropomorphic fingers, SNN receives feedback from neuromorphic sensors, which usually respond to the flexion angle and the force applied to the fingertips. The robotic fingers and hands are in relative motion with the robot's body, which typically includes the neural control unit (NCU) for the limb's motion control. Taking into account that due to the motion of the robotic hands the distance and alignment between the neural modules can vary significantly, we can use VLC technology to implement communication between neurons. In this work, we evaluated for the first time the optical wireless connections between neuromorphic sensors and sSNN for implementing the NCU. The parallel communication between neurons is performed by the recently introduced optical axons which are tolerant to the changes of optical signal intensity due to relative motions of the neural areas. In this experimental setup, we used wavelength division multiplexing to parallelize the operation of axons when each sensor has an associated wavelength. The influence of the optical connections on the robotic arm behaviour was determined by monitoring the sensors' output during steady state for different channels' conditions. The experimental results show that despite small oscillations of the finger force the robotic hand can hold on to an object while moving in the vicinity of NCU.

This document is based upon work from COST Action NEWFOCUS, supported by COST (European Cooperation in Science and Technology)

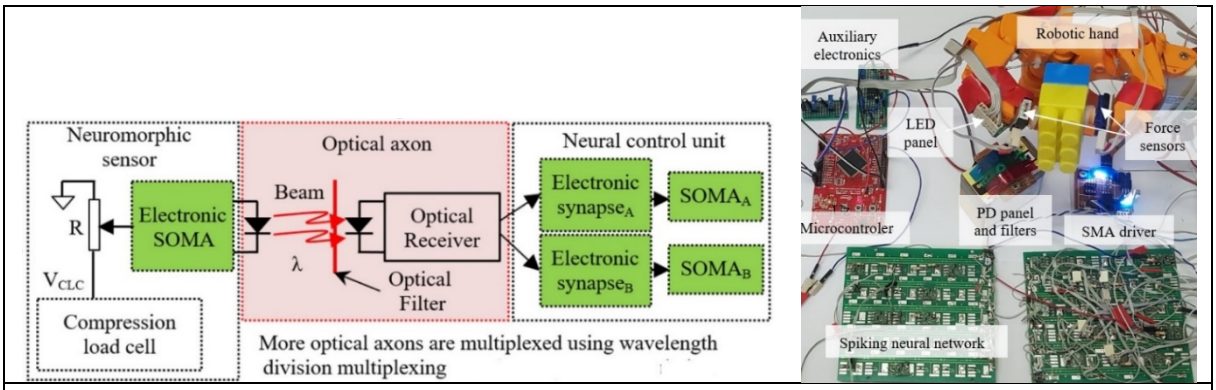

Figure 5. The structure of the neuromorphic sensors with VLC and a picture of the experimental setup.

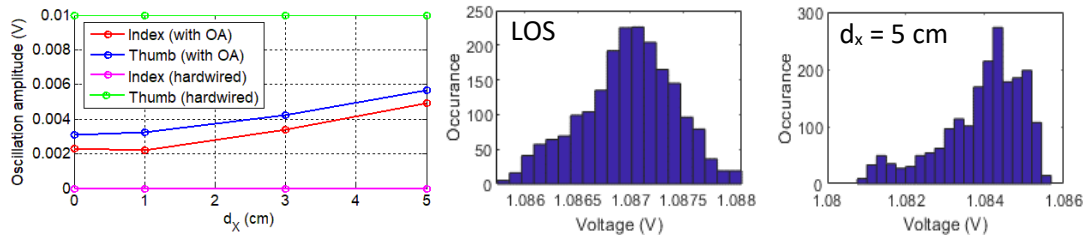

Figure 6. The results showing: (a) the variation of the sensors output with the deviation from the line of sight (LOS); and (b) histograms of the output of the CLC connected to the index finger when optical Rx is placed in the LOS and maximum deviation, respectively.

3.4 Characterization of a perovskites photovoltaic-based optical Rx

The use of photovoltaic (PV) cells for simultaneous energy harvesting and optical detection has remained largely unexplored mostly due to the inherent low bandwidth of PV cells. However, the development of new PV cells based on Perovskite has opened up a window of opportunity for the use of PV as a photodetector (PD) in certain applications. In this work, we investigate flexible Perovskite PV cells as a PD for use in optical wireless communication and characterize it in terms of spectral response, external and power conversion efficiencies, and bandwidth. The results show a maximum responsivity of 0.043 (A/W) at a wavelength of 495 nm, and bandwidth of ~24 and 70 KHz for the active areas of 4 and 0.49 mm^2 , respectively. We demonstrate that the perovskite PD is a promising candidate for energy harvesting and optical detection, thus paving the way for the development of wearable devices in many practical applications. We developed a wearable optical Rx based on the characterized PV cell. Finally, it was proposed a use case for visible light positioning for wearables. The optical link achieves around 5.7 m. The following figure presents the deployed system.

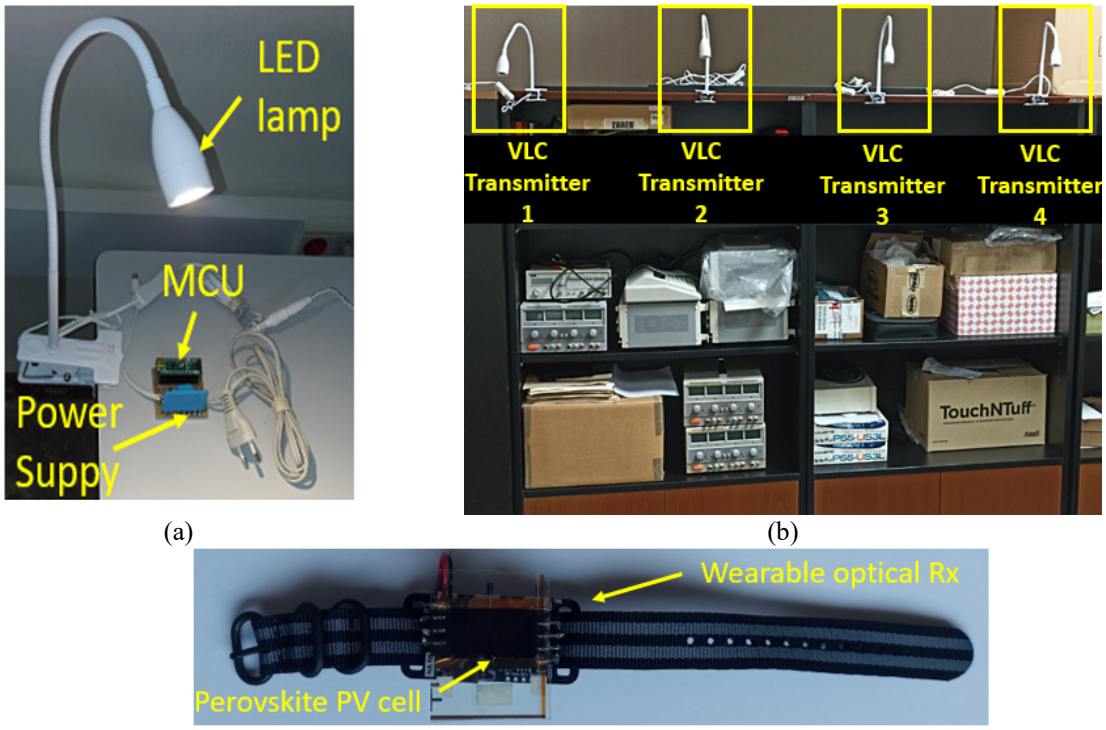

(a) (b)

(c)

Figure 7. (a) Optical Tx based on LED lamp, LED driver and microcontroller ; (b) set of optical Tx to carry out tests ; and (c) wearable based on Perovskite PV cell for indoor positioning.

3.5 Electro-optical SNN using an enhanced optical axon with PAM and automatic gain controller

Visible light communication can be leveraged to establish a wireless link between neurons in spiking networks even when neural areas are in relative motions. In electro-optical spiking neural networks (SNN), parallel transmission can commonly be achieved through wavelength division multiplexing (WDM). However, WDM can be prohibitive in some applications because of the requirement of multiple narrow-band Txs and Rxs with band-pass optical filters. Instead of WDM, this work explores the possibility of using non-orthogonal multiple access (NOMA) in optical axons (OAs) to achieve parallel neural paths in a SNN. To evaluate NOMA based method, we implement an electro-optical SNN that controls the force of two anthropomorphic fingers actuated by the shape memory alloy-based actuators. The signals generated by OAs are multiplexed by the amplitudes of optical pulses, and an additional reference channel is used to dynamically adjust the optical Rx's gain to improve the Rx's decoding performance. The results demonstrated that the influence of the proposed OA on the regulatory performance of the SNN depends on the physical displacement of the OR relative to the Tx. However, this influence did not affect the ability of the robotic arm to hold the object when OPL and deviation vary in certain limits.

This document is based upon work from COST Action NEWFOCUS, supported by COST (European Cooperation in Science and Technology)

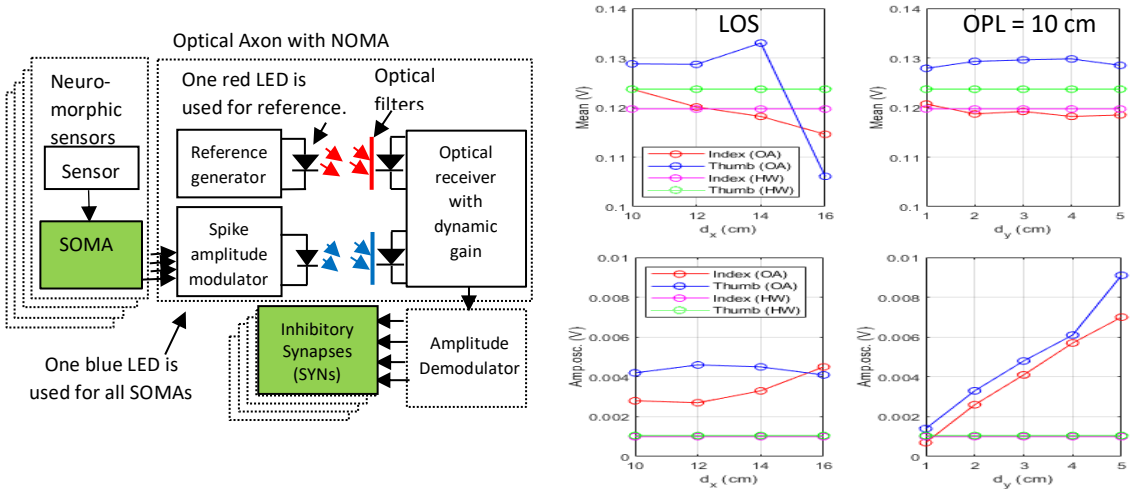

Figure 8 The structure of the optical axon with NOMA and the main results showing the mean and oscillation amplitude of the sensors' output for several values of OPL (dx) and deviation to the side (dy)

References

[1] H.V. Baghdasaryan, T.M. Knyazyan, T.T. Hovhannisyan, G.R. Mardoyan, T. Baghdasaryan, E.Leitgeb, and M.Marciniak.:Reflective Type Multi-Nanolayer Electro-Optical Modulator for Free Space Chip-to-Chip Optical Interconnection: ElectromagneticModelling by the Method of Single Expression, ICTON 2023, We.D1.5, 4 pages. **IEEE Xplore.** https://doi.org/ 10.1109/ICTON59386.2023.10207221

[2] H. Baghdasaryan, T. Knyazyan, T. Hovhannisyan, G. Mardoyan, T. Baghdasaryan, H. Danchov Ivanov, P. Bekhrad, M. Marciniak, E. Leitgeb:Transmission Type Nano-Layered Electro-Optical Modulator for Chip-to-Chip Optical Interconnection:Electromagnetic Modelling by the Method of Single Expression, CoBCom 2022, July 12-14, 2022, 5 pages, Graz, Austria. **IEEE Xplore. https://** doi.org/10.1109/COBCOM55489.2022.9880646

[3] H.V. Baghdasaryan, T.M.Knyazyan, T.T. Hovhannisyan, G. Mardoyan, M. Marciniak, T. Baghdasaryan: Spatial Hole Burning in Reflective Semiconductor Optical Amplifier: Numerical Analysis from the Standpoint of Classical Electromagnetism, 2023 International Workshop on Fiber Optics on Access Networks (FOAN), pp. 23-26,Gent, Belgium.**IEEE Xplore. https://**doi: 10.1109/FOAN59927.2023.10328111.

[4] L. Rodrigues, M. Figueiredo, and L. N. Alves, "Optimized analog multi-band carrierless amplitude and phase modulation for visible light communication-based internet of things systems," Sensors, vol. 21, no. 7, 2021.

[5] L. Rodrigues, M. Figueiredo, L. N. Alves, and Z. Ghassemlooy, "Experimental validation of analog m-cap Rxs for internet of things," in 2022 13th International Symposium on Communication Systems, Networks and Digital Signal Processing (CSNDSP), 2022, pp. 26–31.

[6] L. Rodrigues, M. Figueiredo, L. N. Alves, and Z. Ghassemlooy, "Carrier synchronisation in multiband carrierless amplitude andphase modulation for visible light communication-based iot systems," IET Optoelectronics, vol. 17, no. 4, pp. 120–128, 2023. [Online]. Available: https://ietresearch.onlinelibrary.wiley.com/doi/abs/10.1049/ote2.12095.